

## Article

# Transformation of Glass Fiber Waste into Mesoporous Zeolite-Like Nanomaterials with Efficient Adsorption of Methylene Blue

Cheng-Kuo Tsai <sup>1,2,\*</sup> and Jao-Jia Horng <sup>1,2</sup>

<sup>1</sup> Department of Safety Health and Environmental Engineering, National Yunlin University of Science and Technology, Yunlin 64002, Taiwan; horngjj@gmail.com

<sup>2</sup> Emergency Toxic Response Information Center, National Yunlin University of Science and Technology, Yunlin 64002, Taiwan

\* Correspondence: cksai@yuntech.edu.tw; Tel.: +886-5-5342601 (ext. 4491)

**Abstract:** Recycling and reusing glass fiber waste (GFW) has become an environmental concern, as the means of disposal are becoming limited as GFW production increases. Therefore, this study developed a novel, cost-effective method to turn GFW into a mesoporous zeolite-like nanomaterial (MZN) that could serve as an environmentally benign adsorbent and efficient remover of methylene blue (MB) from solutions. Using the Taguchi optimizing approach to hydrothermal alkaline activation, we produced analcime with interconnected nanopores of about 11.7 nm. This MZN had a surface area of 166 m<sup>2</sup> g<sup>-1</sup> and was negatively charged with functional groups that could adsorb MB ranging from pH 2 to 10 and all with excellent capacity at pH 6.0 of the maximum Langmuir adsorption capacity of 132 mg g<sup>-1</sup>. Moreover, the MZN adsorbed MB exothermically, and the reaction is reversible according to its thermodynamic parameters. In sum, this study indicated that MZN recycled from glass fiber waste is a novel, environmentally friendly means to adsorb cation methylene blue (MB), thus opening a gateway to the design and fabrication of ceramic-zeolite and tourmaline-ceramic balls and ceramic ring-filter media products. In addition, it has environmental applications such as removing cation dyes and trace metal ions from aqueous solutions and recycling water.

**Keywords:** glass fiber waste; hydrothermal alkaline activation; mesoporous zeolite; adsorption capacity; methylene blue



**Citation:** Tsai, C.-K.; Horng, J.-J. Transformation of Glass Fiber Waste into Mesoporous Zeolite-Like Nanomaterials with Efficient Adsorption of Methylene Blue. *Sustainability* **2021**, *13*, 6207. <https://doi.org/10.3390/su13116207>

Academic Editors: Valentina Rognoli and Carla Langella

Received: 1 April 2021  
Accepted: 24 May 2021  
Published: 31 May 2021

**Publisher's Note:** MDPI stays neutral with regard to jurisdictional claims in published maps and institutional affiliations.



**Copyright:** © 2021 by the authors. Licensee MDPI, Basel, Switzerland. This article is an open access article distributed under the terms and conditions of the Creative Commons Attribution (CC BY) license (<https://creativecommons.org/licenses/by/4.0/>).

## 1. Introduction

Glass fiber (GF) is commonly used as a reinforcement material, heat resistor, or stiffness filler in a wide variety of industries, such as renewable energy (wind turbines) [1], electronics (printed circuit boards) [2], automotive [3], aircraft, and aerospace [4]. Growth in the global glass fiber market is incremental, with a 4% rise expected for the period 2019–2024 [5]. As a large amount of waste is generated from these manufacturing processes, disposing of GF waste in an environmentally sound manner has now become a serious issue. The development of a novel nanomaterial composed of glass fiber waste (GFW) should be seen as a sustainable mainstream economic and ecological means of reducing resource consumption and conserving energy. Hence, the previous studies related to this field have prepared porous material from glass-based waste, such as waste-derived mesoporous aluminosilicate (MAS) nanomaterial fabricated from TFT-LCD panel waste, to be used as a carrier to recover boron [6]. Additionally, mesoporous aluminosilicate composite (M-ANC) was developed and used as an adsorbent to capture toxic heavy-metal ions in an aqueous solution [7]. Porous ceramic has been produced from GFW with clay to remove organic dye in an aqueous solution [8]. Those materials were developed through melting and calcination under a high temperature of more than 673 K.

Organic dyes are commonly used for various industrial purposes, which has led to a growing environmental concern over phototoxicity and bioaccumulation [9]. A soluble dye

usually forms a variety of ionic dyestuffs quickly in water, but this dye can also reduce the photosynthetic activities of hydrophytes and pose a possible hazard to human [10–12] and aquatic life [13]. Several techniques have been developed to remove dyes from wastewater: bioremediation, chemical precipitation, oxidation, and adsorption [14]. Adsorption is regarded as effective and economical due to its low cost, toxic tolerance, simple design, and ease of operation [10,15].

To date, there has been a growing tendency to use silica-based mesoporous materials to adsorb dyes in wastewater because of their large surface area, porosity, ordered framework, and thermal stability. For instance, Tran et al. [16] studied the feasibility of nanoparticles derived from zeolite-imidazolate-framework-8 (ZIF8) to remove methyl orange (MO). The result was high adsorption efficiency through electrostatic hydrogen bonding and  $\pi$ - $\pi$  interaction-stacking. Wang et al. [17] synthesized silica-coated  $\text{Fe}_3\text{O}_4$  magnetic nanospheres as adsorbents for congo red (CR) wastewater treatment. The maximum adsorption capacity of this composite adsorbent was  $55 \text{ mg g}^{-1}$  via electrostatic interactions. Qin et al. [18] prepared mesoporous silica nanoparticles (MSNs) to remove cationic dyes in aqueous solution. The results showed that the high adsorption capacities ( $14.7$ – $34.2 \text{ mg g}^{-1}$ ) were because of electrostatic interactions that attracted cationic dyes on the MSN surface. The silica-based porous material has been reported to enhance the efficiency of organic dye removal through grafted functional groups or the incorporation of species on the surface [19–21]. Unfortunately, surface modification generally has a high cost, complicated synthesis procedure, and low yield. Therefore, it is imperative that greener and more economically suitable silica-based mesoporous material adsorbents be fabricated from waste material using a systemic statistical approach.

The Taguchi method, an orthogonal array design combined with statistical analysis and engineering practice, is widely applied in the material manufacturing fields to determine optimum process parameters, such as sintering [22], milling [23], casting [24], and melting [25]. The above studies showed that the Taguchi approach could be efficiently applied to solving process parameters, improving product quality, [26] and reducing energy consumption and pollutant emissions [25]; however, little attention has been paid to the use of zeolite-like mesoporous material from GFW. A Taguchi optimization study like this should reduce energy consumption in resource-related industries. Several studies have been conducted to investigate the optimum process parameters to enhance adsorption capacity to remove methylene blue [27] and optimize Pb(II) ion adsorption on nanohydroxyapatite adsorbents [28]. However, different parameters (reaction agent ratio, temperature, time, and agent concentration) significantly affect the quality of the material process, which affects the efficiency of organic dye removal. The use of an exclusive orthogonal array to reduce the number of experiments, reduce resource consumption, and improve material quality is one of the most pressing issues of our time.

In this study, the chemical composition of GFW is an aluminosilicate glass system, similar to Ca–Mg aluminosilicate stone wool fiber, but with less alkali content. Its surface layer has significant dissolution rates with sodium-based lung fluid and preferential leaching of matrix at the low pH of 4.5 [29]. Therefore, this study proposed transforming a valuable waste from the glass fibers into mesoporous zeolite-like nanomaterial (MZN) to adsorb methylene blue in an aqueous solution. The GFW surface layer could expect higher dissolution rates with an alkali solution that would enhance reactions at 423 K and then apply the low pH to the leaching of the sodium aluminosilicate matrix to produce hydroxyl groups and porosity on the surface to improve adsorption efficiency. The environmental effects of pH, initial concentration, and temperature, were investigated on MB dye's adsorption by GFW and MZN. The adsorption isotherm and kinetics showed that MZN had a higher adsorption capacity toward MB dye removal due to its high surface area and a hydroxyl functional group, and negatively charged sites, creating an accessible electrostatic attraction. Moreover, the regeneration reusability of the MB removal in aqueous solutions proves the potentiality of utilizing MZN as a novel mesoporous adsorbent for environmental applications to remove the organic dye better.

## 2. Materials and Methods

### 2.1. Reagents

Sodium hydroxide (NaOH) and sodium carbonate (Na<sub>2</sub>CO<sub>3</sub>) were obtained from Sigma Aldrich Merck Co. Hydrochloric acid (EL grade) was obtained from BASF Co. Methylene blue C<sub>16</sub>H<sub>18</sub>N<sub>3</sub>ClS was from Panreac Quimica SA. The industrial glass fiber (GFW) is a pure aluminosilicate containing 69.8 wt% SiO<sub>2</sub>, 13.1 wt% Al<sub>2</sub>O<sub>3</sub>, 15.7 wt% CaO, and 0.64 wt% MgO by the ASTM C169-16 method in this study, and the appearance is needle-like with a diameter of about 11–13 μm. The GFW was initially obtained from the local glass fiber manufacturer (Yunlin, Taiwan) in the absence of plastic polymer resin organic matter. It required no further treatment before it was used.

### 2.2. Fabrication of MZN by Taguchi Experimental Design

The controllable factors selected for the fabrication of zeolite-like mesoporous from glass fiber and the effect of four important controllable factors are given in Table S1. Table S2 indicates the fabrication of zeolite-like mesoporous conditions and the MB removal efficiency with an L9 orthogonal array designed by Taguchi methodology. After the hydrothermal reaction, the material was washed several times with 0.1 M HCl until reaching a pH of 7–8.

The experimental results were evaluated by signal-to-noise (*S/N*) ratio divided into three parts: (a) nominal is best, (b) higher is better, and (c) lower is better [30]. As the aim of the investigation into the optimal fabrication of MZN conditions was to achieve the highest possible adsorption capacity of MB, the optimal factors of the process parameters were chosen following larger—the better-quality characteristics. The *S/N* ratio was calculated using Equation (1).

$$S/N = -10 \log_{10} \left[ \frac{1}{n} \sum_{i=1}^n \left( \frac{1}{q_e^2} \right) \right] \quad (1)$$

where *S/N* is the calculated signal-to-noise ratio for the orthogonal L9 array design experiment, *n* is the repetitions number under the same experimental conditions, and *q<sub>e</sub>* represents the results of MB adsorption capacity. The adsorption behavior of MB by L9 experiments mesoporous MZN materials at 298 K and at pH 6.0 was studied, respectively. The initial concentration of MB was 200 mg L<sup>-1</sup>, and the dosage of adsorbent was 1 g L<sup>-1</sup> for 1 h. The MB adsorption capacity was calculated using Equation (2).

$$q_e = \frac{(C_0 - C_e)}{m} \times V \quad (2)$$

where *C*<sub>0</sub>, *C<sub>e</sub>*, denote the MB initial concentration (mg L<sup>-1</sup>) and equilibrium concentration (mg L<sup>-1</sup>), and *V*, *m* denotes the solution volume (L) and the mesoporous MZN materials mass (g) [31].

### 2.3. Characterization

The morphology and the cross-sectional image of zeolite-like materials were examined by FE-SEM (JEOL JSM 7610F Plus) at 15 kV and HR-TEM (JEOL JEM-2100 Plus) at 200 kV. The aluminosilicate materials cross-section was prepared by the rotary microtome (Leica Ultracut). The crystallinity of the sample was obtained by an X-ray diffractometer (XRD) using a Bruker D825A advanced with Cu Kα in a wavelength of 1.5405 Å at the voltage and current density of 40 kV and 40 mA, respectively. The change in relation to the element's composition in zeolite-like mesoporous material was assessed using an X-ray photoelectron spectrometer (XPS, PHI 5000 VersaProbe III). Besides, the Brunauer–Emmett–Teller (BET)-specific surface area, and the pore property determination of the GFW and MZN materials were performed using a Micrometrics ASAP 2020 analyzer under the nitrogen adsorption–desorption isotherms at 77 K. ASTM C169-16 was used to the quantify metal oxide components in GFW and MZN. The zeta potential measurement was measured

utilizing a Malvern instrument Zetasizer Nano ZS to inspect the before and after activation materials' surface behavior in each pH point.

#### 2.4. Adsorption of MB onto Mesoporous Zeolite-Like Nanomaterials

The adsorption isotherm experiment was performed with silicate-based materials of MB using batch experiments. After adding 0.5 g L<sup>-1</sup> adsorbent GFW and MZN to the solutions with the various initial MB concentration ranging from 0–150 mg g<sup>-1</sup> at pH 6.0, effect of pH (2–10) and adsorption thermodynamics in the temperature range of 288 K to 318 K were investigated. In addition, the experiments for kinetics were carried out using 200 mg·L<sup>-1</sup> MB solution, and the adsorbent dosage is 1.0 g L<sup>-1</sup>. This solution was shaken at various intervals in the range of 0–120 min. Moreover, batches were shaken at 120 r.p.m for 24 h under isothermally at 298 K in the dark. The residual concentration of MB was determined at a maximum absorbance wavelength of 665 nm by using a UV-vis spectrophotometer (U-2900, Hitachi) [32].

#### 2.5. Thermal Reusability Study

After the adsorption experiment was completed, the MZN adsorbent was prepared by calcination in an atmosphere at 773 K and held for 2 h when it reached 773 K. After MZN cooling, 1.0 g L<sup>-1</sup> MZN was then agitated with 100 mL of 200 mg L<sup>-1</sup> MB solution for 2 h adsorption experiments again. The regeneration experiments were carried out in five successive cycles.

### 3. Result and Discussion

#### 3.1. Optimization Using Taguchi Approach

This study set out to develop the optimal parameters for the fabrication of mesoporous zeolite-like material, using the Taguchi method to enhance the adsorption capacity of MB from wastewater. The signal-to-noise ratio was employed to evaluate the high-quality properties deviating from the target value. The adsorption capacity values and *S/N* ratio for each experiment are given in Table 1, which provides the effect of each control factor on the response, and Figure 1 shows the main forces plot for the *S/N* ratio. The optimum conditions are clearly illustrated as follows: (1) activating agent ratio (*w/w*) was 1:10; (2) agent concentration was 2.5 M; (3) the hydrothermal temperature was 423 K; and (4) hydrothermal time was 16 h. Based on the fabrication of MZN parameters affecting the adsorption capacity of the MB removal in the aqueous solution, the activating agent ratio and the hydrothermal time were observed to be the most dominant, as shown in Table 2. This was mainly due to the ranks derived from the delta values compared to the relative magnitude of effects [33].

**Table 1.** L9 orthogonal array for MB adsorption capacity (*q<sub>e</sub>*) and signal-to-noise ratio.

Factors				<i>q<sub>e</sub></i> (mg g <sup>-1</sup> )	<i>S/N</i> Ratio
Agent Ratio ( <i>w/w</i> )	Agent Conc. (M)	Temp. (K)	Time (HR)		
1:2.5	1	393	8	36.6	31.28
1:2.5	2.5	423	16	114	41.18
1:2.5	5	453	24	88.1	38.90
1:5	1	423	24	107	40.58
1:5	2.5	453	8	84.6	38.54
1:5	5	393	16	114	41.15
1:10	1	453	16	106	40.53
1:10	2.5	393	24	111	40.93
1:10	5	423	8	103	40.27

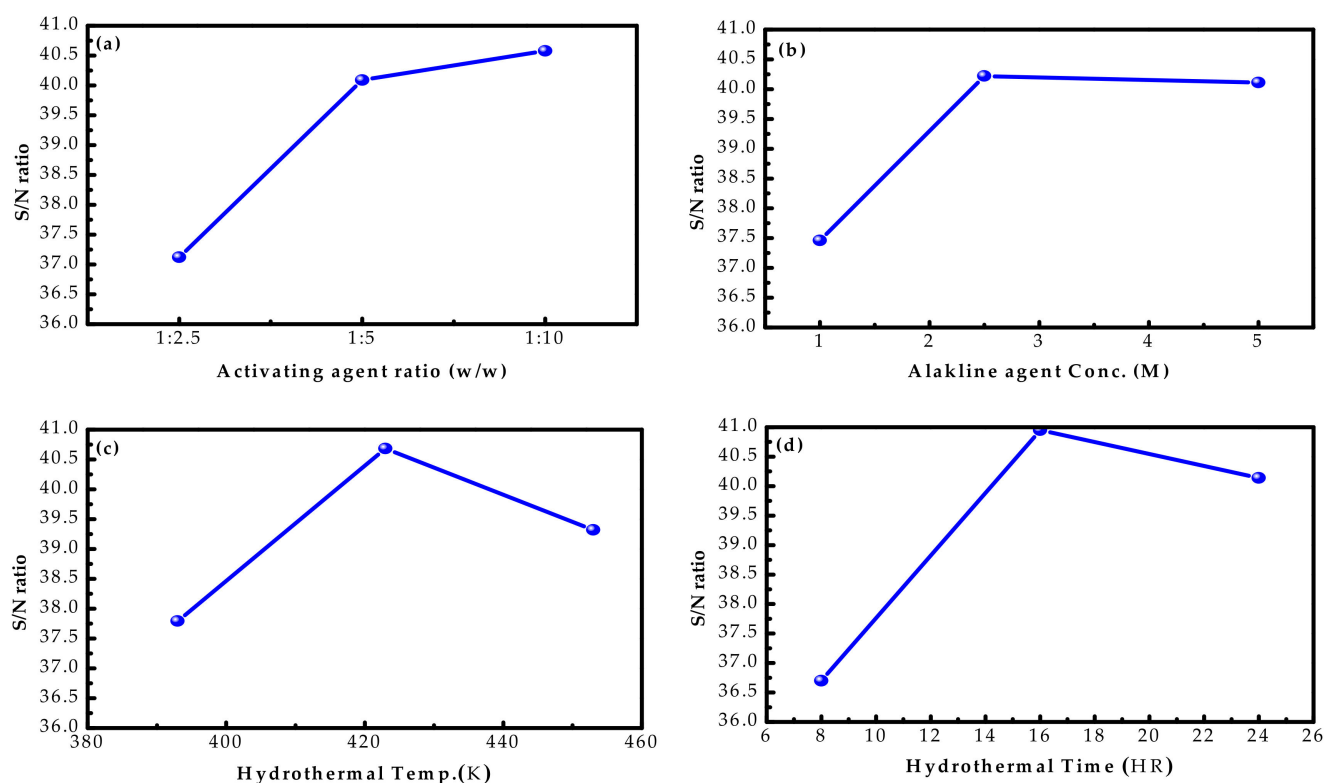


**Figure 1.** Mean of  $S/N$  ratios were calculated and plotted against four factors activating agent ratio (a), activating agent Conc. (b), hydrothermal temp. (c), and time (d) with three levels.

**Table 2.** Average of the response characteristic at each level of the factor for  $S/N$  ratios (higher is better).

Level	Agent Ratio ( $w/w$ )	Agent Conc. (M)	Temp. (K)	Time (HR)
L1	37.12	37.46	37.79	36.7
L2	40.09	40.22	40.68	40.95
L3	40.58	40.11	39.32	40.14
Delta	3.46	2.75	2.89	4.25
Rank	2	4	3	1

Herein, the activating agent ratio and activation time are the most critical factors for the hydrothermal-alkaline reaction because of its having a significant tunneling effect on cleavage of the tetrahedrally coordinated cages of Si-O-Si linkage connected via bridging oxygens (BO) into reactive Si-O<sup>-</sup> clusters, where an alkali metal cation establishes charge neutrality for the negatively charged nonbridging oxygens (NBOs) [34], resulting in getting a high surface area with functional activate sites on the mesoporous zeolite-like surface. Therefore, the MB adsorption capacity of the mesoporous zeolite-like nanomaterial under the optimized reaction parameters has been shown by Taguchi methods. The optimized condition for the high adsorption capacity of MB removal in the aqueous solution was confirmed experimentally. The results showed that the high adsorption capacity of MB as 120 mg g<sup>-1</sup> was more excellent than all the other experimental runs. Additionally, the standard deviation obtained from the validation experiment was 2.1. This was based on the validation experiments performed ten times (Table S3, Supplementary data). This part of the results implies the precision of the optimization procedure. However, surface morphology, pore texture, adsorption isotherm, and kinetics of the mesoporous zeolite-like material were investigated.

### 3.2. Surface Characterization of Mesoporous Zeolite-Like Nanomaterial

The surface morphology of glass fiber waste and as-prepared MZN was first characterized and compared by electronic microscopic images. Figure 2a shows the original glass fiber SEM image showed a coarse rod-like fiber pattern on a uniform surface. According to the SEM images of MZN in Figure 2b–d, the replacement material structure framework showed the growth of a needle-like cilium crystalline structure and presented many flake crystal phases with a multi-layered assembly. They intertwined with each other to form a porous structure.

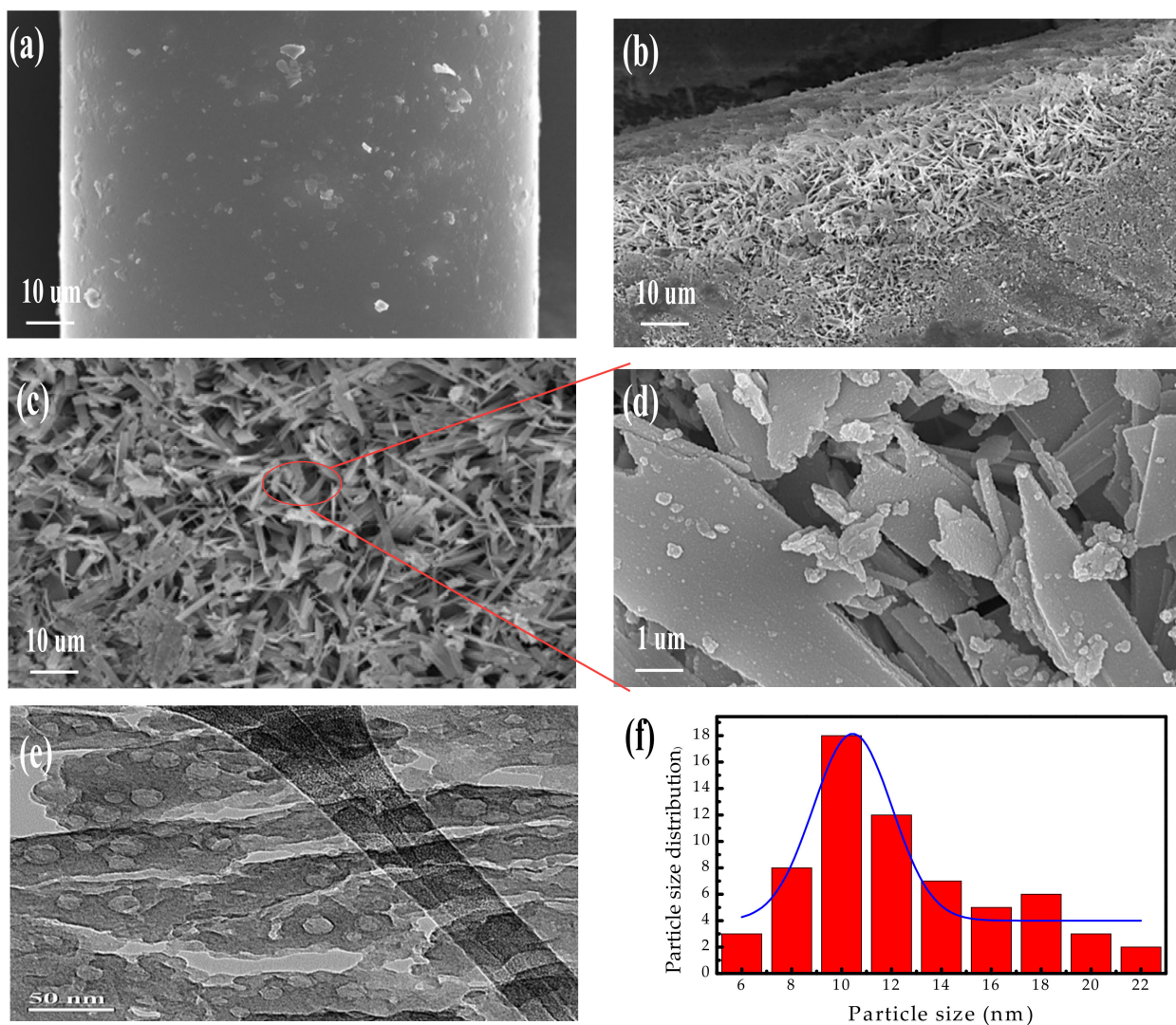


**Figure 2.** The SEM images of GFW (a) and (b–d) MZN nanomaterial of different scale, (e) cross sectional HR-TEM image of MZN, and (f) particle size distribution of MZN.

Moreover, for the cross-sectional HR-TEM image of MZN, as shown in Figure 2e, a wide range of nanostructured pores appeared in the internal layer structure of MZN. Besides, the MZN showed the homogeneous distribution of nanoparticles on the surface, which forms a hierarchical structure of glass fiber after NaOH hydrothermal activation and 0.1 M HCl acid leaching. As illustrated in Figure 2f, the distribution of MZN particles exhibits a narrow particle size range of 6–22 nm with an average size of  $11.7 \pm 3.6$  nm ( $n = 64$ ). This hierarchical structure could provide a sizeable specific area and valuable sites to serve as an adsorbent for the adsorption of MB dye from wastewater to better purifying aqueous quality. It is noted that our previous study used glass base waste material to

prepare the mesoporous aluminosilicate using alkaline activation. The mean particle size was 12.8 nm after melting at more than 800 °C [6], confirming that a novel mesoporous material could develop at a lower temperature with hydrothermal reaction.

The crystallinity of GFW and MZN was further identified using XRD. Figure 3a exhibits the XRD patterns of glass fiber waste before and after activation treatment. The XRD patterns of the GFW showed several peaks located in the  $2\theta$  of 20.8°, 26.6°, 36.5°, 50.1°, 59.9° and 68.1°, which could be assigned as the (100), (101), (110), (112), (211), and (203) planes of quartz, syn  $\text{SiO}_2$  (JCPDS 46-1045). Moreover, the XRD pattern of MZN after activation treatment in the presence of NaOH showed several peaks at shifts 15.8°, 18.2°, 24.2°, 25.9°, 30.5°, 31.9°, 33.2°, 35.8°, 37.0°, 40.45, and 47.7°, which could be assigned as the (211), (202), (312), (400), (332), (422), (501), (512), (404), (611), and (604) planes of analcime zeolite-like material (JCPDS 19-1180). It is noteworthy that the fabrication of analcime zeolite from glass fiber waste without template was observed, which agrees well with those reported studies by Liu et al. [35,36]. This is mainly because the glass fibers were extremely fast quenched (cooling rate > 105 K/s), and their network structure possesses much higher potential energy [37]. The glass fiber of quartz  $\text{SiO}_2$  is more easily alkali-activated to a breaking reaction between the Si-O and Al-O bond under the hydrothermal process at a low temperature of 423 K. This improvement reactivity and provision of Na ions was concentrated on the surface of the particles [38]. For this reason, it seems that quartz  $\text{SiO}_2$  can play a favorite role in dissolved into free Si-O tetrahedron to form analcime  $\text{Na}(\text{AlSi}_2\text{O}_6)\cdot\text{H}_2\text{O}$  [39] with the enriched  $\text{Na}^+$  around the particles.

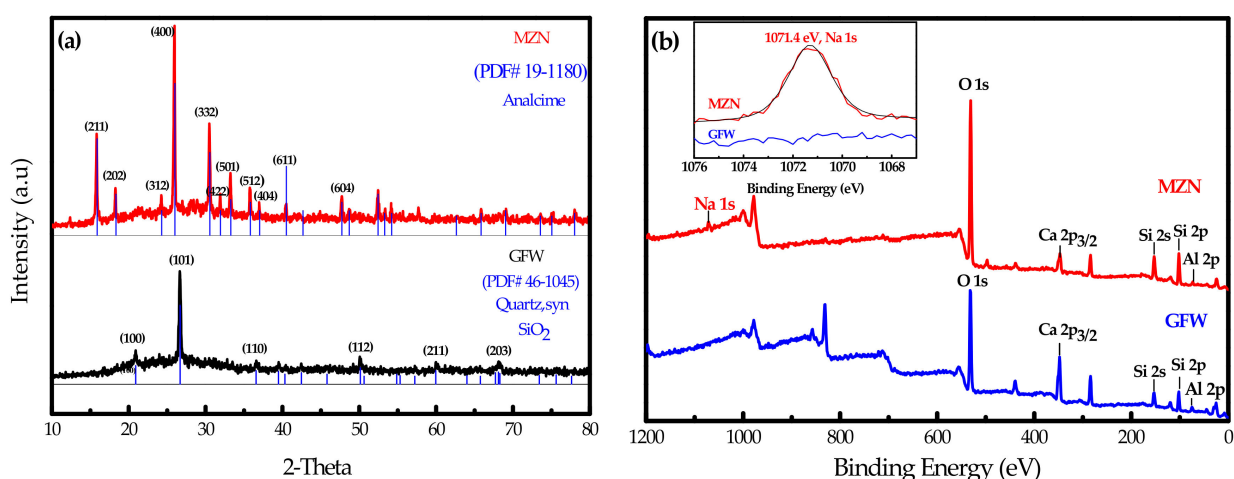


**Figure 3.** (a) XRD patterns of GFW and MZN, (b) XPS spectra of GFW and MZN, inset in (b) is the enlarged figure of Na 1s peak of GFW and MZN.

GFW dominant constituents were found to be 69.8 wt%  $\text{SiO}_2$ , 13.1 wt%  $\text{Al}_2\text{O}_3$ , and 15.7 wt% CaO with the alkali-free glass fiber. The compositions of mesoporous zeolite-like nanomaterial slightly increased after the alkaline activation, and the weight percentages of  $\text{SiO}_2$ ,  $\text{Al}_2\text{O}_3$ , CaO, and  $\text{Na}_2\text{O}$  accounted for 58.4, 15.3, 17.0, and 6.80 wt%, respectively, in MZN (Table S4, Supplementary data). The slight decrease in  $\text{SiO}_2$  was mainly attributed to the fact that the alkali activation with the high-pressure system under 423 K caused the dissolution of  $\text{SiO}_2$  during the acid-washing procedure, which is similar to our previous result [7]. In contrast, the addition of NaOH alkaline reaction increased the  $\text{Na}_2\text{O}$  components after activation.

To further study the surface chemistry of the GFW and MZN, the XPS spectra of GFW and the activation treatment of MZN materials were determined (Figure 3b). Several XPS peaks shows the Al 2p, Si 2p, Si 2s, Ca 2p<sub>3/2</sub>, O 1s, and Na 1s at 75, 102, 153, 348, 532, and 1071 eV, respectively. As clearly illustrated in the Figure 3b inset, the addition of NaOH was followed by the hydrothermal treatment appearance. Therefore, the Na peaks at 1071 eV increased the oxygen intensity at O 1s peak in the MZN. This result is well in line with

the result of analcime zeolite obtained by XRD analysis. When the original GFW reacted with NaOH during the activation of hydrothermal treatment, the quartz phase through the induced transformation to form the crystalline aluminosilicate framework, and the exposure of oxygen atoms would produce Si-OH or Si-O $\cdots$ Na $^+$  groups [40]. Therefore, the quartz SiO $_2$  in the GFW could be completely tailored as the analcime zeolite after the alkaline reaction.

### 3.3. The Pore Texture of Mesoporous Zeolite-Like Nanomaterials

The specific surface area and pore texture of the original GFW and MZN were further examined. As shown in Figure 4a, the nitrogen adsorption–desorption isotherm of GFW showed a quantity of weakly adsorbed capacity following type IV isotherm with a hysteresis loop in the relative pressure range ( $P/P_0$ ) of 0.55–0.99. The specific surface area of the original GFW was 11.2 m $^2$  g $^{-1}$ , which results obtained were close to the original superfine glass fiber [41]. In contrast to the original GFW materials, the MZN material also followed type IV physisorption behavior with a strongly H3 hysteresis loop intensity in the relative pressure ( $P/P_0$ ) range of 0.4–0.99. This was mainly contributed from the capillary condensation in mesoporous structure [42,43], which could benefit and provide a large surface area of the adsorption for dye macromolecules. Hence, the specific surface area increased from 11.2 m $^2$  g $^{-1}$  of the original GFW material to 166 m $^2$  g $^{-1}$  for MZN after the alkaline activation (Table S5, Supplementary data) higher than the report result of analcime zeolite [44]. Nasser et al. [45] fabricated the analcime phase zeolite of aluminum isopropoxide, using the hydrothermal method, by sodium hydroxide and aluminum sources. They found that the specific surface area was 20.2 m $^2$  g $^{-1}$ . Abdelrahman et al. [46] also prepared an analcime/sodium aluminum silicate using hydrothermal by Si(IV) template mixture at 393 K for one day. They found that the specific surface area of the dried analcime/sodium aluminum silicate hydrate was 12.7 m $^2$  g $^{-1}$ . In this study, a novel MZN material of the specific surface area was 8.2–13.0 times higher than those reported data. It is presumably attributed to the alkaline through breaking the Si-O and Al-O bond of quartz SiO $_2$  structure into free Si-O tetrahedron to form analcime and the inter-connected pore size.

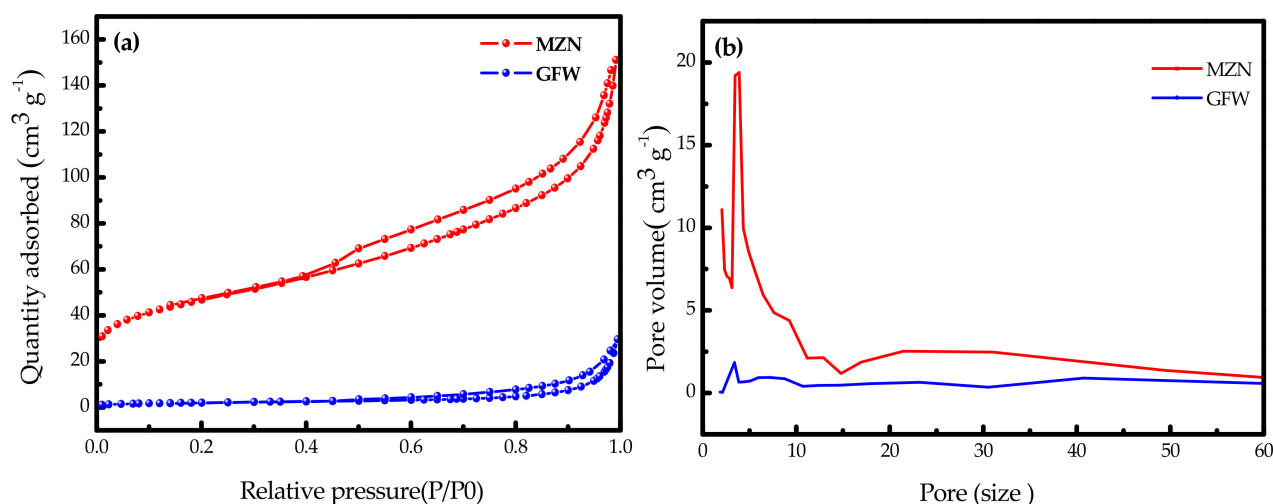


**Figure 4.** BET surface area (a) and pore size distribution (b) of the original (GFW) and activated mesoporous zeolite-like nanomaterial (MZN).

Besides, the MZN pore size distribution exhibited a sharp peak at 3.8 nm. It gradually produced the second peak and the third one in the range of 8.0–15 nm. Finally, a broad pore size distribution in the mesoporous region (15–50 nm) followed (Figure 4b). Moreover, the mean pore size diameter of the MZN is around 7.3 nm. According to Liu et al. [35], they synthesized analcime zeolite from waste fly ash (SiO $_2$ /Al $_2$ O $_3$  = 4.0) after geopolymerization

and hydrothermal with alkaline reaction. They found that the pore size distribution was in the range of 7.7–9.9 nm, which is in fair agreement with our results.

### 3.4. Adsorption of Methylene Blue by MZN

#### 3.4.1. Effect of pH

The adsorption capacity of activated mesoporous zeolite-like nanomaterial (MZN) was first evaluated by the adsorption of methylene blue organic solutions at pH 2–10. Figure 5a displays the adsorption capacity of methylene blue (MB) by MZN as a pH function. The removal efficiency of MB increased rapidly with the increase in the pH ranging from 2.0 to 6.0, and then slowly increased pH from 6.0 to 10. This part of the results corroborates those results derived from the studies performed using different silica-based [47] and biochar/iron oxide composites [48] as the adsorbent. The isoelectric point ( $pH_{IEP}$ ) of MZN materials was identified. As illustrated in Figure 5b, the  $pH_{IEP}$  of untreated glass fiber (GFW) was 6.5 and then shifted to 2.0 after alkaline activation. It is noteworthy that the MZN surface was negatively charged in the pH range of 2.0–10, thereby indicating the excellent removal performance of MZN toward the cationic dye through the electrostatic interaction. The negatively charged mesoporous surface could enhance the adsorption capacity of MZN toward cationic dye of MB adsorption. In addition, the large amount of  $H^+$  in low pH could compete with  $MB^+$  for exchange sites in zeolite [35]. It is noteworthy that the MZN nanomaterial surface contains negatively charged ions exchange sites with a high surface area, which would be a significant reaction mechanism for the removal of cationic dyes pollutant in aqueous solutions. Therefore, further experiments should be selected at pH 6.0 to investigate the adsorption behavior of methylene blue by MZN nanomaterials and the thermodynamic investigation into this regard.

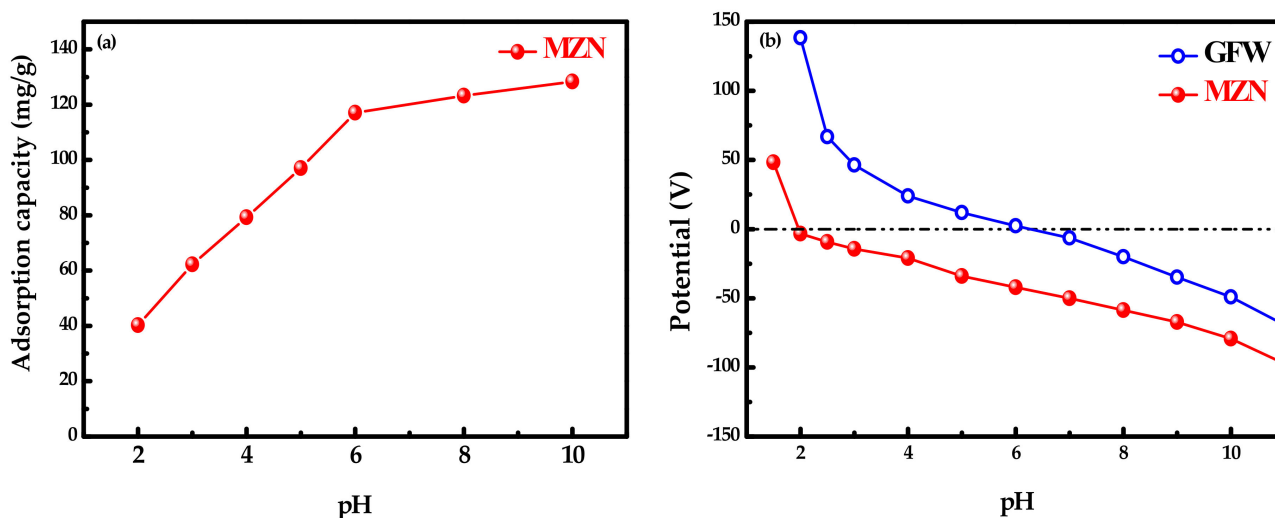


**Figure 5.** (a) Adsorption capacity of mesoporous MZN materials toward MB adsorption at different pH and (b) isoelectric point of GFW and MZN materials as a function of pH.

#### 3.4.2. Adsorption Isotherm of MB by MZN

The adsorption behavior of MB by original waste material (GFW) and mesoporous MZN materials at 298 K and pH 6.0 was studied, as given in Figure 6a. The GFW had low adsorption capacity toward MB adsorption as  $10 \text{ mg g}^{-1}$ , and this change was probably attributed to the high  $pH_{IEP}$  and the lower specific surface of GFW. MZN was an extraordinary adsorbent toward MB adsorption in comparison with GFW. The adsorption capacity of MB using MZN increased dramatically at a low equilibrium concentration of  $<20 \text{ mg L}^{-1}$  and then leveled off to the plateau in the high equilibrium concentration ranging from 40 to  $120 \text{ mg L}^{-1}$ .

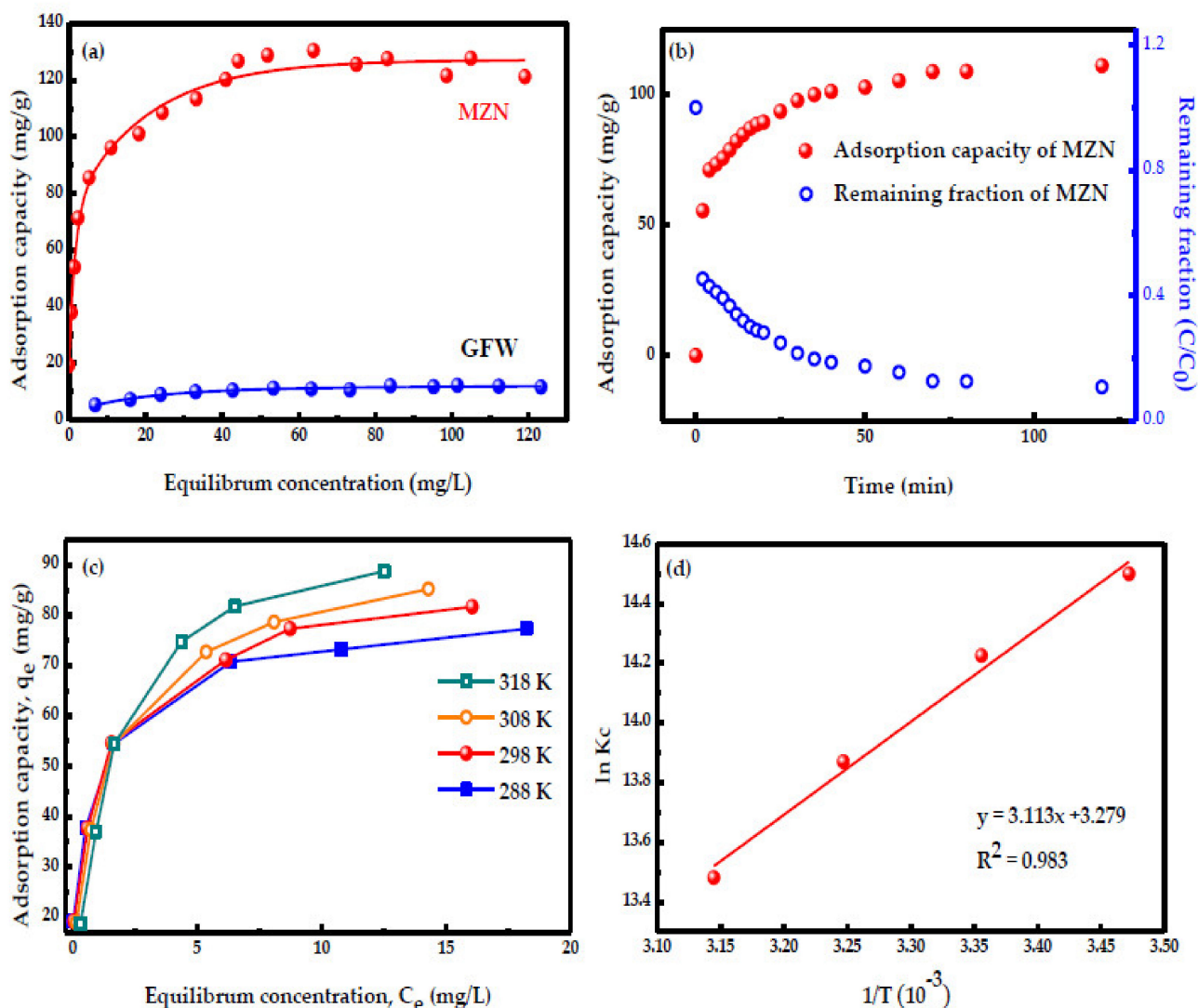


**Figure 6.** (a) Adsorption isotherms of MB dye adsorbed onto GFW and MZN in aqueous solutions and (b) adsorption kinetic of MB dye adsorbed onto MZN at pH 6.0. (c) Adsorption isotherms of MB dye adsorbed onto MZN at various temperatures, and (d) plot of  $\ln K_c$  vs.  $1/T$  for MB adsorption onto MZN. The initial concentration of MB is 10–60 mg L<sup>-1</sup>, the adsorbent dosage is 1 g L<sup>-1</sup>, and the adsorption time is 60 min.

The adsorption isotherm study can describe the affinity and the adsorption behavior of MB on the surface of adsorbents. Therefore, the adsorption isotherm model of MB onto MZN was investigated, using Langmuir and Freundlich isotherm models of Equations (3) and (4), respectively.

$$\frac{C_e}{q_e} = \frac{1}{K_L q_m} + \frac{C_e}{q_m} \quad (3)$$

$$q_e = K_F C_e^{\frac{1}{n}} \quad (4)$$

The Langmuir adsorption isotherm can well describe the adsorption isotherms of MB, and the fitted parameters of Langmuir and Freundlich models were shown in (Table S6, Supplementary data). The Langmuir isotherm model could accurately describe the adsorption capacity of MB using MZN, and the correlation coefficients ( $R^2$ ) were more than 0.995. It implies that monolayer sorption proceeds over a surface containing a limited number of adsorption sites and uniform adsorption strategies with no emigration of adsorbate in the extension of a surface [10]. Moreover, the maximum adsorption capacity of MB is 132 mg g<sup>-1</sup>. A previous study used the alkali-fused rice straw biochar to adsorb MB, and

the study revealed that the adsorption capacity was close to  $132 \text{ mg g}^{-1}$  [47], which lends support to our results. Due to negatively charged surface it could adsorb cationic ion of MB more readily to adsorb onto the MZN surface.

Table 3 shows a comparison of the adsorption capacity of MB by MZN with the reported data obtained from the various silica-based adsorbents. The reported adsorption capacity for MB by a wide variety of silica-based adsorbents, including PVDF/glass as-prepared composite membrane [49], silica xerogel [27], pure silica [50], hollow silica [51], Ag/SiO<sub>2</sub> [52], and hydroxyl group silica aerogel [53], were in the range of 44.4–102  $\text{mg g}^{-1}$ , respectively. In this study, the adsorption capacity of MB by MZN is better than most of the reported silica-based adsorbents, indicating that MZN is an excellent negative charged material for effective adsorption of positive charged MB in an aqueous solution. The surface modification, grafting, and cross-linking with functionalized groups were employed to enhance the active sites and increase the adsorption performance [54–56]. Yang et al. (2019) developed a novel of montmorillonite (Mt) with graphene oxide (GO) composite by grafting with 3-aminopropyl triethoxysilane (APTES) for MB removal and found that maximum adsorption capacity was  $471 \text{ mg g}^{-1}$  because of the reaction between MB and oxygenic groups of GO to form Mt and graphene oxide nanosheets. Brião et al. [56] proposed a novel method to convert biopolymers into ZSM-5 zeolites through facile strategies, creating a large surface area, large pore volumes and improving the adsorption capacity  $115 \text{ mg g}^{-1}$  for MB at 298 K. Khanday et al. [56] reviewed and summarized the adsorption of MB by zeolite/chitosan (Z-AC/C) cross-linked composite. They found that the maximum adsorption capacity of MB by chitosan-functionalized was  $152 \text{ mg g}^{-1}$ . In this study, a novel MZN can drive electrostatic attraction and high surface area to enhance the adsorption capacity of MB, which is higher than that in most of the reported studies. It indicates the superiority of the analcime zeolite-like composites prepared by recycled glass fiber waste.

**Table 3.** Adsorption performance for MB reported in the literature.

Adsorbent	pH	Surface Area ( $\text{m}^2 \text{ g}^{-1}$ )	Temp. (K)	Adsorption Capacity ( $\text{mg g}^{-1}$ )	Ref.
PVDF/glass as-prepared membrane	7	278	298	44.4	[Zhang et al., 2019]
Silica xerogel	5	195	313	51.9	[Guzel Kaya et al., 2019]
Pure silica	6.5	421	-	102	[Alizadeh Arasi, et al., 2020]
Hollow silica	7	67.0	298	64.0	[Verma, et al., 2020]
Ag/SiO <sub>2</sub>	7	208	-	55.0	[Hu, et al., 2019]
Hydroxyl group silica aerogel	7	628	-	47.2	[Han, et al., 2016]
Montmorillonite/graphene oxide	7	74.6	303	471	[Yang et al., 2019]
Mesoporous zeolite (ZSM-5)	7	164	298	115	[Brião, et al., 2018]
Zeolite/chitosan composite	-	83.0	303	152	[Khanday, et al., 2017]
Mesoporous zeolite-like material	6	166	298	132	This study

### 3.4.3. Adsorption Kinetics

Adsorption kinetic models can describe the solute removal behavior at the liquid-solid interface [48]. Therefore, the pseudo-first-order model, the pseudo-second-order model, and the intra-particle diffusion model were used to investigate the adsorption kinetic model of MB onto MZN. The model parameters from the fitting calculation shown in Table 4. This study observed the kinetic adsorption results of MB onto MZN as a function of time, as presented in Figure 6b. The adsorption capacity increased quickly in the first 5–30 min, and the removal efficiency increased up to 80%. It then gradually leveled off to the maximum adsorption amount, and the amount was  $111 \text{ mg g}^{-1}$  after 40–120 min of adsorption.

**Table 4.** Kinetics model constant for the adsorption of cationic ion MB onto MZN nanocomposite.

Kinetic Model	Equation <sup>a</sup>	Parameters	MB
Adsorbed amount	-	$q_e$ , exp (mg g <sup>-1</sup> ) $q_e$ , cal (mg g <sup>-1</sup> )	111.0 23.8
Pseudo-first order	$\log(q_e - q_t) = \log q_e - k_1 t$	$k_1$ (min <sup>-1</sup> ) $R^2$	0.0046 0.858
Pseudo-second order	$\frac{t}{q_t} = \frac{1}{k_2 q_e^2} + \frac{t}{q_2}$	$q_e$ , cal (mg g <sup>-1</sup> ) $k_2$ (g mg <sup>-1</sup> min <sup>-1</sup> ) $R^2$	113.0 0.0023 0.998
Intra-particle diffusion	$q_t = k_{id} t^{0.5} + C$	$k_{id}$ (mg g <sup>-1</sup> min <sup>0.5</sup> ) $C$ $R^2$	5.12 64.6 0.921

Note: <sup>a</sup>:  $q_e$  is the adsorption capacity at equilibrium,  $q_t$  is the adsorbed amount at time  $t$ ,  $k_1$ , and  $k_2$  are the pseudo-first-order and pseudo-second-order rate constants, respectively,  $k_{id}$  is the intra-particle diffusion rate constant,  $C$  is the intercept, and  $t$  is the adsorption time.

Figure S2 (Supplementary data) shows the plots of  $\log(q_e - q_t)$ ,  $t/q_t$ , and  $q_t$  as an against time ( $t$  or  $t^{0.5}$ ). According to the equation, the rate constant and maximum adsorption capacity was determined from the linearity slope and intercept. Table 4 indicates that the proper pseudo-second-order kinetic model described the adsorption data more accurately than the pseudo-first-order and intra-particle diffusion models because the correlation coefficient  $R^2$  value was as high as 0.998. This might suggest that the pseudo-second-order kinetic model could be suitably used to describe MB's adsorption behavior by MZN. The adsorption mechanism of MZN for the MB solution may play a chemisorption role. Besides, the data fitting result of the intra-particle diffusion model showed the  $R^2$  value of 0.921. This could be described in two linear parts. The first stage was attributed to MB molecules diffusion through the solution into the adsorbents' external surfaces during adsorption times ( $t^{1/2}$ ) in the range of 1–4, while, in contrast, the second stage of time( $t^{1/2}$ ) in the field of 4–10 involved slow intra-particle diffusion into the MZN pores [57,58]. Various kinds of silica-based materials have been reported the similar results that the pseudo-second-order kinetics model is more suitable to describe the adsorption behavior of MB onto adsorbents, including zeolite/chitosan [56], mesoporous zinc silicate composite [58], geopolymer-expanded glass composite [59] and magnetic zeolites [60]. It is noteworthy that the adsorption process can be involves valence forces through sharing or exchange of electrons between adsorbent and adsorbate as covalent forces [58].

#### 3.4.4. Adsorption Thermodynamics

A thermodynamic study of adsorption can effectively describe and exhibit adsorption mechanisms through the adsorption equilibrium experiment under different temperatures [61]. As can be seen from Figure 6c,d, the four different temperatures (288, 298, 308, and 318 K) were set to expand the adsorption isotherms of MB onto MZN, where the experimental data of adsorption equilibrium might be the Langmuir isotherm. Therefore, this study is possibly feasible to apply the Langmuir constant ( $K_L$ ) as the thermodynamic equilibrium constant ( $K_C$ ) so as further to estimate the thermodynamic parameters [62]. Significantly, the relatively high temperature could improve the adsorption capacity of MB (Figure 6c). This might have been due to the enhanced interaction between the active sites with MB molecules when the temperature increased [63]. Commonly, the thermodynamic parameters, including standard Gibbs energy change ( $\Delta G^\circ$ , kJ·mol<sup>-1</sup>), standard enthalpy change ( $\Delta H^\circ$ , kJ·mol<sup>-1</sup>), and standard entropy change ( $\Delta S^\circ$ , J·K<sup>-1</sup>·mol<sup>-1</sup>), were calculated from the following equations [63]:

$$\Delta G^\circ = -RT \ln K_C \quad (5)$$

$$\Delta G^\circ = \Delta H^\circ - T \Delta S^\circ \quad (6)$$

$$\ln K_C = \frac{-\Delta H^\circ}{R} \times \frac{1}{T} + \frac{\Delta S^\circ}{R} \quad (7)$$

where  $R$  is the universal gas constant ( $8.3144 \text{ J/mol} \times \text{K}$ ), and  $T$  is the absolute temperature in Kelvin (K). The Gibbs energy change was directly calculated from Equation (6), while the enthalpy change,  $\Delta H$  ( $\text{KJ mol}^{-1}$ ) and the entropy change,  $\Delta S$  ( $\text{J} \cdot (\text{mol K})^{-1}$ ) were determined from the slope and intercept of the Van't Hoff plots of  $\ln K_C$  against  $1/T$  (Figure 6d). Table S7 shows that the exact values of the thermodynamic parameters.  $\Delta G$  values were more negative and decreased from  $-34.7$  to  $-35.6$  ( $\text{KJ} \cdot \text{mol}^{-1}$ ), with the temperature increasing from 288 to 318 K because the adsorption of MB onto MZN was favorable at higher temperature [64]. Additionally, the value of  $f \Delta H$  ( $25.9 \text{ KJ mol}^{-1}$ ) negatives confirms that the interaction of MB adsorbed by MZN was an exothermic process. This positive entropy change  $\Delta S$  ( $31.0 \text{ J} \cdot (\text{mol K})^{-1}$ ) suggests increased randomness on the surface of the adsorbent–liquid interface with the reversible process, showing an increasing trend during the attachment [65].

### 3.5. Reusability Evaluation of MZN

Five cycles of applications were applied to verify the stability and reusability of the MZN material, as exhibited in Figure 7. The adsorption–desorption experiments were conducted for five cycles through the repeated calcinate of the MZN [10]. Although the removal efficiency of MB onto MZN decreased from 97% to 80% (adsorption capacity 124 to  $102 \text{ mg g}^{-1}$ ) after the 1st use, the effectiveness was stable from 2nd to 5th use. Those possible causes could be the closure of pores due to the sintering effect as the calcination temperature is much higher than the hydrothermal temperature and the desorption of bottleneck effect [63]. Therefore, the adsorption capacity and removal efficiency of this mesoporous MZN were stable after the 1st use with good reusability. However, this MZN will be applied to treat other organic and inorganic pollutants in the future.

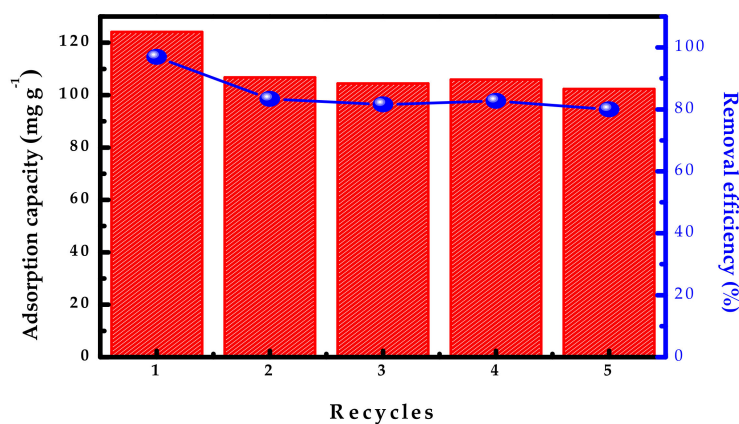


**Figure 7.** Recyclability of MZN for removal of MB (Dosage  $1 \text{ g L}^{-1}$ , initial conc.  $200 \text{ mg L}^{-1}$  for 2 h). **Note.** The bar graph of red color indicates the adsorption capacity of MB; the blue color shows the MB removal efficiency.

## 4. Conclusions

This study successfully developed a novel mesoporous analcime MZN from the glass fiber waste to adsorb MB from solutions effectively. By the Taguchi approach, the optimal production parameters were the activating agent ratio ( $w/w$ ) 1:10, the agent concentration 2.5 M, the hydrothermal temperature 423 K, and the hydrothermal time of 16 h to transform glass fiber wastes create functional nanocomposites of Si-OH or Si-O $\cdots$ Na $^+$  active sites through hydrothermal-alkaline reaction. This MZN has many mesoporous channels and hydroxyl functional groups/negative charged sites on the analcime zeolite surface with a large surface area of  $166 \text{ m}^2 \text{ g}^{-1}$  and particle sizes ranging from 6 to 22 nm. This MZN also exhibited an excellent adsorption capacity toward MB ranging from pH 2 to 10, predominantly attributed to the electrostatic attraction between the negatively charged surfaces on MZN and the positively charged cationic MB $^+$ . The adsorption isotherms could be described by both the Langmuir adsorption isotherm model and the kinetics by the

pseudo-second-order kinetic model. The maximum adsorption capacity was calculated to be  $132 \text{ mg g}^{-1}$  for MB. Moreover, thermodynamic parameters depicted that the reaction was both exothermic and reversible for MB. The reusability of MZN was also tested in five cycles with the removal efficiencies of MB from 97% on the 1st use to about 80% of the 2nd to 5th use. Those results indicated that glass fiber wastes could be effectively transformed into a novel, cost-effective and reusable mesoporous analcime zeolite nanocomposite (MZN) for removing MB in aqueous solutions and maybe other pollutants. As well, this sustainable reusability method being alkali-activation could be a wide range applied to reprocess glasses-based waste (such as waste mineral wool glasses and lamp glasses) to save as an environmentally friendly nanomaterial in the future.

**Supplementary Materials:** The following are available online at <https://www.mdpi.com/article/10.3390/su13116207/s1>, Figure S1. (a) Langmuir and (b) Freundlich adsorption isotherms of MB onto MZN, Figure S2. The (a) pseudo-first-order, (b) pseudo-second-order kinetics, and (c) intra-particle diffusion model of adsorption of MB onto MZN nano-adsorbent, Table S1. Experimental parameters and three levels, Table S2. Fabrication of MZN material orthogonal L9 array for MB sorption, Table S3. Ten-time validation experiments of the optimization procedure, Table S4. Compositions of dominant constituents in GFW and MZN, Table S5. The surface area, pore volume and pore size of the glass fiber waste before (GFW) and after (MZN) the activation process, Table S6. Isotherm parameters of MB adsorption onto the MZN material, Table S7. Thermodynamic parameters for the adsorption of MB on MZN.

**Author Contributions:** Conceptualization, C.-K.T. and J.-J.H.; methodology, C.-K.T. and J.-J.H.; validation, J.-J.H.; formal analysis, C.-K.T. and J.-J.H.; resources, J.-J.H.; data curation, C.-K.T.; writing—original draft preparation, C.-K.T.; writing—review and editing, J.-J.H.; visualization, C.-K.T. and J.-J.H.; funding acquisition, J.-J.H. All authors have read and agreed to the published version of the manuscript.

**Funding:** Ministry of Science and Technology (MOST), Taiwan, for the financial support under Grant No. 109-2221-E-224-021.

**Institutional Review Board Statement:** Not applicable.

**Informed Consent Statement:** Not applicable.

**Data Availability Statement:** The data presented in this study are available on request from the corresponding author.

**Acknowledgments:** The authors would like to express special thanks to the Ministry of Science and Technology (MOST), Taiwan, for the financial support under Grant No. 109-2221-E-224-021.

**Conflicts of Interest:** The authors declare no conflict of interest.

## References

1. Liu, P.; Meng, F.; Barlow, C.Y. Wind turbine blade end-of-life options: An eco-audit comparison. *J. Clean. Prod.* **2019**, *212*, 1268–1281. [[CrossRef](#)]
2. Wang, Y.; Zou, B.; Yin, G. Wear mechanisms of Ti (C7N3)-based cermet micro-drill and machining quality during ultra-high speed micro-drilling multi-layered PCB consisting of copper foil and glass fiber reinforced plastics. *Ceram. Int.* **2019**, *45*, 24578–24593. [[CrossRef](#)]
3. Joo, S.-J.; Yu, M.-H.; Kim, W.S.; Lee, J.-W.; Kim, H.-S. Design and manufacture of automotive composite front bumper assemble component considering interfacial bond characteristics between over-molded chopped glass fiber polypropylene and continuous glass fiber polypropylene composite. *Compos. Struct.* **2020**, *236*, 111849. [[CrossRef](#)]
4. Zabihi, O.; Ahmadi, M.; Nikafshar, S.; Preyeswary, K.C.; Naebe, M. A technical review on epoxy-clay nanocomposites: Structure, properties, and their applications in fiber reinforced composites. *Compos. Part B Eng.* **2018**, *135*, 1–24. [[CrossRef](#)]
5. Nechifor, G.; Totu, E.E.; Nechifor, A.C.; Constantin, L.; Constantin, A.M.; Cărauşu, M.E.; Isildak, I. Added value recyclability of glass fiber waste as photo-oxidation catalyst for toxic cytostatic micropollutants. *Sci. Rep.* **2020**, *10*, 1–16. [[CrossRef](#)] [[PubMed](#)]
6. Tsai, C.-K.; Lee, N.-T.; Huang, G.-H.; Suzuki, Y.; Doong, R.-A. Simultaneous recovery of display panel waste glass and wastewater boron by chemical oxo-precipitation with fluidized-bed heterogeneous crystallization. *ACS Omega* **2019**, *4*, 14057–14066. [[CrossRef](#)] [[PubMed](#)]
7. Tsai, C.-K.; Doong, R.-A.; Hung, H.-Y. Sustainable valorization of mesoporous aluminosilicate composite from display panel glasses waste for adsorption of heavy metal ions. *Sci. Total Environ.* **2019**, *673*, 337–346. [[CrossRef](#)]

8. Yasui, K.; Sasaki, K.; Ikeda, N.; Kinoshita, H. Dye adsorbent materials based on porous ceramics from glass fiber-reinforced plastic and clay. *Appl. Sci.* **2019**, *9*, 1574. [[CrossRef](#)]
9. Ahmad, R.; Guo, J.; Kim, J. Structural characteristics of hazardous organic dyes and relationship between membrane fouling and organic removal efficiency in fluidized ceramic membrane reactor. *J. Clean. Prod.* **2019**, *232*, 608–616. [[CrossRef](#)]
10. Pan, X.; Zhang, M.; Liu, H.; Ouyang, S.; Ding, N.; Zhang, P. Adsorption behavior and mechanism of acid orange 7 and methylene blue on self-assembled three-dimensional MgAl layered double hydroxide: Experimental and DFT investigation. *Appl. Surf. Sci.* **2020**, *522*, 146370. [[CrossRef](#)]
11. Li, Y.; Wu, M.; Wang, B.; Wu, Y.; Ma, M.; Zhang, X. Synthesis of magnetic lignin-based hollow microspheres: A highly adsorptive and reusable adsorbent derived from renewable resources. *ACS Sustain. Chem. Eng.* **2016**, *4*, 5523–5532. [[CrossRef](#)]
12. Domingues, J.T.; Orlando, R.M.; Millán, R.D.S.; García, A.D.P.; Rodrigues, G.D. Polymer-bixin nanofibers: A promising environmentally friendly material for the removal of dyes from water. *Sep. Purif. Technol.* **2020**, *248*, 117118. [[CrossRef](#)]
13. Aslam, S.; Subhan, F.; Yan, Z.; Yaseen, M.; Shujahat, M.H. Fabrication of gold nanoparticles within hierarchically ZSM-5-based micro-/mesostructures (MMZ) with enhanced stability for catalytic reduction of p-nitrophenol and methylene blue. *Sep. Purif. Technol.* **2021**, *254*, 117645. [[CrossRef](#)]
14. Grover, A.; Mohiuddin, I.; Malik, A.K.; Aulakh, J.S.; Kim, K.-H. Zn-Al layered double hydroxides intercalated with surfactant: Synthesis and applications for efficient removal of organic dyes. *J. Clean. Prod.* **2019**, *240*, 118090. [[CrossRef](#)]
15. Xie, H.; Zhang, J.; Wang, D.; Liu, J.; Wang, L.; Xiao, H. Construction of three-dimensional g-C<sub>3</sub>N<sub>4</sub>/attapulgite hybrids for Cd (II) adsorption and the reutilization of waste adsorbent. *Appl. Surf. Sci.* **2020**, *504*, 144456. [[CrossRef](#)]
16. Tran, V.A.; Kadam, A.N.; Lee, S.-W. Adsorption-assisted photocatalytic degradation of methyl orange dye by zeolite-imidazole-framework-derived nanoparticles. *J. Alloys Compd.* **2020**, *835*, 155414. [[CrossRef](#)]
17. Wang, P.; Wang, X.; Yu, S.; Zou, Y.; Wang, J.; Chen, Z.; Alharbi, N.S.; Alsaedi, A.; Hayat, T.; Chen, Y. Silica coated Fe<sub>3</sub>O<sub>4</sub> magnetic nanospheres for high removal of organic pollutants from wastewater. *Chem. Eng. J.* **2016**, *306*, 280–288. [[CrossRef](#)]
18. Qin, P.; Yang, Y.; Zhang, X.; Niu, J.; Yang, H.; Tian, S.; Zhu, J.; Lu, M. Highly efficient, rapid, and simultaneous removal of cationic dyes from aqueous solution using monodispersed mesoporous silica nanoparticles as the adsorbent. *Nanomaterials* **2018**, *8*, 4. [[CrossRef](#)]
19. Han, H.; Rafiq, M.K.; Zhou, T.; Xu, R.; Mašek, O.; Li, X. A critical review of clay-based composites with enhanced adsorption performance for metal and organic pollutants. *J. Hazard. Mater.* **2019**, *369*, 780–796. [[CrossRef](#)]
20. Zhou, Y.; Lu, J.; Zhou, Y.; Liu, Y. Recent advances for dyes removal using novel adsorbents: A review. *Environ. Pollut.* **2019**, *252*, 352–365. [[CrossRef](#)]
21. Meng, S.; Yu, S.; Tang, F.; Hu, X.; Lu, J.; Fei, X.; Zhu, M. Fiber engineering of silica-based aerogels with surface specificity and regenerability for continuous removal of dye pollutants from wastewaters. *Microporous Mesoporous Mater.* **2021**, *314*, 110874. [[CrossRef](#)]
22. Dingal, S.; Pradhan, T.; Sundar, J.S.; Choudhury, A.R.; Roy, S. The application of Taguchi's method in the experimental investigation of the laser sintering process. *Int. J. Adv. Manuf. Technol.* **2008**, *38*, 904–914. [[CrossRef](#)]
23. Zhang, J.Z.; Chen, J.C.; Kirby, E.D. Surface roughness optimization in an end-milling operation using the Taguchi design method. *J. Mater. Process. Technol.* **2007**, *184*, 233–239. [[CrossRef](#)]
24. Sushil, K.; Satsangi, P.; Prajapati, D. Optimization of green sand casting process parameters of a foundry by using Taguchi method. *Int. J. Adv. Manuf. Technol.* **2010**, *55*, 23–34.
25. Wang, J.-M.; Yan, H.-J.; Zhou, J.-M.; Li, S.-X.; Gui, G.-C. Optimization of parameters for an aluminum melting furnace using the Taguchi approach. *Appl. Therm. Eng.* **2012**, *33*, 33–43. [[CrossRef](#)]
26. Thakker, M.R.; Parikh, J.K.; Desai, M.A. Synergism between ionic liquid and ultrasound for greener extraction of geraniol: Optimization using different statistical tools, comparison and prediction. *Chem. Eng. Res. Des.* **2018**, *134*, 162–171. [[CrossRef](#)]
27. Guzel Kaya, G.; Yilmaz, E.; Devci, H. A novel silica xerogel synthesized from volcanic tuff as an adsorbent for high-efficient removal of methylene blue: Parameter optimization using Taguchi experimental design. *J. Chem. Technol. Biotechnol.* **2019**, *94*, 2729–2737. [[CrossRef](#)]
28. Googerdchian, F.; Moheb, A.; Emadi, R.; Asgari, M. Optimization of Pb (II) ions adsorption on nanohydroxyapatite adsorbents by applying Taguchi method. *J. Hazard. Mater.* **2018**, *349*, 186–194. [[CrossRef](#)]
29. Barly, S.H.; Okhrimenko, D.V.; Solvang, M.; Yue, Y.; Stipp, S.L. Dissolution of Stone Wool Fibers with Phenol-urea-formaldehyde Binder in a Synthetic Lung Fluid. *Chem. Res. Toxicol.* **2019**, *32*, 2398–2410. [[CrossRef](#)]
30. Zolfaghari, G.; Esmaili-Sari, A.; Anbia, M.; Younesi, H.; Amirmahmoodi, S.; Ghafari-Nazari, A. Taguchi optimization approach for Pb (II) and Hg (II) removal from aqueous solutions using modified mesoporous carbon. *J. Hazard. Mater.* **2011**, *192*, 1046–1055. [[CrossRef](#)]
31. Shahabuddin, S.; Tashakori, C.; Kamboh, M.A.; Korrani, Z.S.; Saidur, R.; Nodeh, H.R.; Bidhendi, M.E. Kinetic and equilibrium adsorption of lead from water using magnetic metformin-substituted SBA-15. *Environ. Sci. Water Res. Technol.* **2018**, *4*, 549–558. [[CrossRef](#)]
32. Guo, D.; Li, Y.; Cui, B.; Hu, M.; Luo, S.; Ji, B.; Liu, Y. Natural adsorption of methylene blue by waste fallen leaves of Magnoliaceae and its repeated thermal regeneration for reuse. *J. Clean. Prod.* **2020**, *267*, 121903. [[CrossRef](#)]
33. Nia, P.M.; Jenatabadi, H.S.; Woi, P.M.; Abouzari-Lotf, E.; Alias, Y.J.M. The optimization of effective parameters for electrodeposition of reduced graphene oxide through Taguchi method to evaluate the charge transfer. *Measurement* **2019**, *137*, 683–690.

34. Ning, C.; Hadi, P.; Xu, M.; Lin, C.S.K.; McKay, G. Valorization of an electronic waste-derived aluminosilicate: Surface functionalization and porous structure tuning. *ACS Sustain. Chem. Eng.* **2016**, *4*, 2980–2989. [[CrossRef](#)]
35. Liu, Z.; Li, L.; Shao, N.; Hu, T.; Han, L.; Wang, D. Geopolymerization enhanced hydrothermal synthesis of analcime from steel slag and CFBC fly ash and heavy metal adsorption on analcime. *Environ. Technol.* **2020**, *41*, 1753–1765. [[CrossRef](#)]
36. Bortolini, H.R.; Lima, D.S.; Perez-Lopez, O.W. Hydrothermal synthesis of analcime without template. *J. Cryst. Growth* **2020**, *532*, 125424. [[CrossRef](#)]
37. Ya, M.; Deubener, J.; Yue, Y. Enthalpy and anisotropy relaxation of glass fibers. *J. Am. Ceram. Soc.* **2008**, *91*, 745–752. [[CrossRef](#)]
38. Zhang, Y.; Jing, Z.; Kameda, T.; Yoshioka, T. Hydrothermal synthesis of hardened diatomite-based adsorbents with analcime formation for methylene blue adsorption. *RSC Adv.* **2016**, *6*, 26765–26774. [[CrossRef](#)]
39. Hameed, A.M.; Alharbi, A.; Abdelrahman, E.A.; Mabrouk, E.; Hegazey, R.; Algethami, F.K.; Al-Ghamdi, Y.O.; Youssef, H.M. Facile hydrothermal fabrication of analcime and zeolite x for efficient removal of Cd (II) ions from aqueous media and polluted water. *J. Inorg. Organometallic Polym. Mater.* **2020**, *30*, 4117–4128. [[CrossRef](#)]
40. Kazemian, H.; Naghdali, Z.; Kashani, T.G.; Farhadi, F. Conversion of high silicon fly ash to Na-P1 zeolite: Alkaline fusion followed by hydrothermal crystallization. *Adv. Powder Technol.* **2010**, *21*, 279–283. [[CrossRef](#)]
41. Wang, F.; Yu, J.; Liang, X.; Lu, S.; Liu, Z.; Liu, L. Effect of heat treatment on the morphology, diameter and mesoporous of superfine glass fiber. *J. Text. Inst.* **2020**, *112*, 123–131. [[CrossRef](#)]
42. You, S.-M.; Tasi, C.-K.; Millet, P.; Doong, R.-A. Electrochemically capacitive deionization of copper (II) using 3D hierarchically reduced graphene oxide architectures. *Sep. Purif. Technol.* **2020**, *251*, 117368. [[CrossRef](#)]
43. Li, K.; Yu, L.; Cai, J.; Zhang, L.J.M. Removal of dyes from aqueous solution using novel C@C composite adsorbents. *Microporous Mesoporous Mater.* **2021**, *313*, 110840. [[CrossRef](#)]
44. Youssef, H.M.; Shah, R.K.; Algethami, F.K.; Hegazey, R.; Naglah, A.M.; Al-Omar, M.A.; Alluhaybi, A.A.; Alherbish, H.A.; Mabrouk, E.; Abdelrahman, E.A. Facile hydrothermal procedure for the synthesis of sodium aluminum silicate hydrate/analcime and analcime for effective removal of manganese (II) ions from aqueous solutions. *J. Inorg. Organometallic Polym. Mater.* **2020**, *31*, 1035–1046. [[CrossRef](#)]
45. Nassar, M.Y.; Abdelrahman, E.A. Hydrothermal tuning of the morphology and crystallite size of zeolite nanostructures for simultaneous adsorption and photocatalytic degradation of methylene blue dye. *J. Mol. Liq.* **2017**, *242*, 364–374. [[CrossRef](#)]
46. Abdelrahman, E.A.; Alharbi, A.; Subaihi, A.; Hameed, A.M.; Almutairi, M.A.; Algethami, F.K.; Youssef, H.M. Facile fabrication of novel analcime/sodium aluminum silicate hydrate and zeolite Y/faujasite mesoporous nanocomposites for efficient removal of Cu (II) and Pb (II) ions from aqueous media. *J. Mater. Res. Technol.* **2020**, *9*, 7900–7914. [[CrossRef](#)]
47. Wang, K.; Peng, N.; Sun, J.; Lu, G.; Chen, M.; Deng, F.; Dou, R.; Nie, L.; Zhong, Y. Synthesis of silica-composited biochars from alkali-fused fly ash and agricultural wastes for enhanced adsorption of methylene blue. *Sci. Total Environ.* **2020**, *729*, 139055. [[CrossRef](#)]
48. Zhang, P.; O'Connor, D.; Wang, Y.; Jiang, L.; Xia, T.; Wang, L.; Tsang, D.C.; Ok, Y.S.; Hou, D. A green biochar/iron oxide composite for methylene blue removal. *J. Hazard. Mater.* **2020**, *384*, 121286. [[CrossRef](#)]
49. Zhang, Y.; Liu, J.; Du, X.; Shao, W. Preparation of reusable glass hollow fiber membranes and methylene blue adsorption. *J. Eur. Ceram. Soc.* **2019**, *39*, 4891–4900. [[CrossRef](#)]
50. Alizadeh Arasi, M.; Salem, A.; Salem, S. Extraction of nano-porous silica from hydrosodalite produced via modification of low-grade kaolin for removal of methylene blue from wastewater. *J. Chem. Technol. Biotechnol.* **2020**, *95*, 1989–2000. [[CrossRef](#)]
51. Verma, M.; Dwivedi, P.K.; Saxena, N.J.C. Hollow silica nanoparticles synthesized from core-shell nanoparticles as highly efficient adsorbent for methylene blue and its invitro release: Mechanism and Kinetics study. *Colloids Surf. A Physicochem. Eng. Asp.* **2020**, *587*, 124333. [[CrossRef](#)]
52. Hu, M.; Yan, X.; Hu, X.; Feng, R.; Zhou, M. Synthesis of silver decorated silica nanoparticles with rough surfaces as adsorbent and catalyst for methylene blue removal. *J. Sol-Gel Sci. Technol.* **2019**, *89*, 754–763. [[CrossRef](#)]
53. Han, H.; Wei, W.; Jiang, Z.; Lu, J.; Zhu, J.; Xie, J. Removal of cationic dyes from aqueous solution by adsorption onto hydrophobic/hydrophilic silica aerogel. *Colloids Surf. A Physicochem. Eng. Asp.* **2016**, *509*, 539–549. [[CrossRef](#)]
54. Yang, Y.; Yu, W.; He, S.; Yu, S.; Chen, Y.; Lu, L.; Shu, Z.; Cui, H.; Zhang, Y.; Jin, H. Rapid adsorption of cationic dye-methylene blue on the modified montmorillonite/graphene oxide composites. *Appl. Clay Sci.* **2019**, *168*, 304–311. [[CrossRef](#)]
55. Brião, G.V.; Jahn, S.L.; Foletto, E.L.; Dotto, G.L. Highly efficient and reusable mesoporous zeolite synthesized from a biopolymer for cationic dyes adsorption. *Colloids Surf. A Physicochem. Eng. Asp.* **2018**, *556*, 43–50. [[CrossRef](#)]
56. Khanday, W.; Asif, M.; Hameed, B. Cross-linked beads of activated oil palm ash zeolite/chitosan composite as a bio-adsorbent for the removal of methylene blue and acid blue 29 dyes. *Int. J. Biol. Macromol.* **2017**, *95*, 895–902. [[CrossRef](#)] [[PubMed](#)]
57. Sumalinog, D.A.G.; Capareda, S.C.; de Luna, M.D.G. Evaluation of the effectiveness and mechanisms of acetaminophen and methylene blue dye adsorption on activated biochar derived from municipal solid wastes. *J. Environ. Manag.* **2018**, *210*, 255–262. [[CrossRef](#)]
58. Dong, G.; Tian, G.; Gong, L.; Tang, Q.; Li, M.; Meng, J.; Liang, J. Mesoporous zinc silicate composites derived from iron ore tailings for highly efficient dye removal: Structure and morphology evolution. *Microporous Mesoporous Mater.* **2020**, *305*, 110352. [[CrossRef](#)]
59. Rożek, P.; Król, M.; Mozgawa, W. Lightweight geopolymer-expanded glass composites for removal of methylene blue from aqueous solutions. *Ceram. Int.* **2020**, *46*, 19785–19791. [[CrossRef](#)]

60. Supelano, G.; Cuaspud, J.G.; Moreno-Aldana, L.C.; Ortiz, C.; Trujillo, C.; Palacio, C.; Vargas, C.P.; Gómez, J.M. Synthesis of magnetic zeolites from recycled fly ash for adsorption of methylene blue. *Fuel* **2020**, *263*, 116800. [[CrossRef](#)]
61. Tran, H.N.; You, S.-J.; Chao, H.-P. Thermodynamic parameters of cadmium adsorption onto orange peel calculated from various methods: A comparison study. *J. Environ. Chem. Eng.* **2016**, *4*, 2671–2682. [[CrossRef](#)]
62. Milonjić, S.K. A consideration of the correct calculation of thermodynamic parameters of adsorption. *J. Serb. Chem. Soc.* **2007**, *72*, 1363–1367. [[CrossRef](#)]
63. Huang, T.; Yan, M.; He, K.; Huang, Z.; Zeng, G.; Chen, A.; Peng, M.; Li, H.; Yuan, L.; Chen, G.J. Efficient removal of methylene blue from aqueous solutions using magnetic graphene oxide modified zeolite. *J. Colloid Interface Sci.* **2019**, *543*, 43–51. [[CrossRef](#)]
64. Gal, Y.-S.; Jin, S.-H.; Park, J.W.; Lim, K.T. Comparative study between liquid. liquid extraction and bulk liquid membrane for the removal and recovery of methylene blue from wastewater. *J. Ind. Eng. Chem.* **2015**, *30*, 261–265. [[CrossRef](#)]
65. Maneechakr, P.; Karnjanakom, S. Adsorption behaviour of Fe (II) and Cr (VI) on activated carbon: Surface chemistry, isotherm, kinetic and thermodynamic studies. *J. Ind. Eng. Chem.* **2017**, *106*, 104–112. [[CrossRef](#)]